Journal of Applied Electrochemistry **31**: 1141–1147, 2001.

Electrodeposition of zinc from high acid zinc chloride solutions

D.S. BAIK[1] and D.J. FRAY[2]
[1]*SangWon EnC Ltd, Kangseo-Gu Nebalsan-dong 646-2, Seoul, Republic of Korea*
[2]*Department of Materials Science and Metallurgy, University of Cambridge, Cambridge, Great Britain*

Received 14 August 2000; accepted in revised form 5 June 2001

Key words: gelatin, membrane, zinc chloride, zinc electrodeposition

Abstract

Electrowinning of zinc from zinc chloride solutions, acidified by HCl, was conducted in a cation exchange membrane cell. The current efficiency was correlated with the deposit morphology. The deposits having lesser surface defects, which act as active sites for hydrogen adsorption, exhibited higher current efficiency. The (1 1 0) preferred texture was observed on the deposits grown in high acid solution containing gelatin. High temperature (40 °C) and high current density decreased the current efficiency and the preferred texture.

1. Introduction

One of the reasons why sulfuric acid has been widely used in hydrometallurgical treatment for extraction of zinc from zinc ore or waste is because of the ease of electrowinning zinc from sulfate solutions. However, from the viewpoint of leaching, hydrochloric acid is a very efficient lixivant [1], especially for electric arc furnace dust containing stable zinc ferrite that can only be leached in highly aggressive acidic solutions. In spite of the advantages of the high leaching efficiency and the relatively clean residue, not containing jarosite, it is rarely utilized due to the problems of chloride electrolysis, producing chlorine, which eventually leads the loss of hydrochloric acid. The few studies of zinc electrodeposition in zinc chloride solutions have all produced chlorine gas. Higher solubility and electrical conductivity of $ZnCl_2$ to decrease solution resistance are further advantages over sulfate electrolysis. Utilizing these advantages, Thomas and Fray [2] conducted the electrolysis in high concentration (18–35 wt %) of zinc chloride with high current densities (220–250 mA cm^{-2}) achieving 90% of current efficiency (CE). However, leachate solutions are usually below 18% $ZnCl_2$ which means that lower current density (<100 mA cm^{-2}) have to be used.

Direct electrolysis using an electrowinning cell containing an ion exchange membrane is a possible method for the metal chloride treatment with recovery of hydrochloric acid. In nickel chloride electrolysis [3], a cell divided into three compartments by one anion and one cation exchange membranes has been used to regenerate 1 M HCl. The cell is unsuitable for direct application for Zn electrowinning due to the low current density requiring large areas of the expensive membrane and high cell voltage due to the use of two membranes. A better alternative would be a two-compartment cell divided by a cation exchange membrane. In this case, zinc is deposited at the cathode, oxygen is liberated at the anode and hydrogen ions pass from the anolyte (sulfate solution) to the catholyte (chloride solution) through the cation selective membrane.

With chloride electrolysis producing chlorine at the anode, there is only a modest decrease in the pH of the solution as the zinc concentration of the electrolyte falls. With the membrane cell, the pH of the catholyte can fall quite rapidly as hydrogen ions diffuse into the catholyte that can lead to evolution of hydrogen on the cathode. However, there are also advantages of producing HCl in the catholyte as it raises the conductivity of the electrolyte and produces a low pH leachant.

In the process described here a cell having a cation-exchange membrane was used to obtain high acid solutions from the electrowinning cell that are suitable as leachants. Furthermore, to maximize the extraction yield in the electrolysis cell, it was necessary to manage low Zn concentration. From preliminary investigations, without using air sparging, the dendrite-like deposits were predominant in all the deposits. Dendrites can be avoided by using air sparging but air sparging has undesirable side effects, that is, water and acid loss by evaporation coupled with additional costs for the installation and the maintenance of the sparging line. In high acid solutions, the air sparging would cause toxic atmosphere containing hydrochloric acid. To avoid air sparging, a levelling agent was used. Various kinds of leveling agents including proteinous additives [4] and alkyl ammonium chlorides have already been found to be effective in making dense coatings. Gelatin [5] was well known for the levelling agent in sulfate and in chloride solutions and was used in this work.

2. Experimental details

An H-shaped electrolysis cell divided into two compartments by a membrane (Nafion®-117, DuPont) was used (Figure 1). Two flat glass joints having 4.9 cm^2 of inner circular area were used to insert the membrane. Electrodes were positioned at the centres of each compartment. The platinum-coated titanium anode had 4.9 cm^2 of circular exposed areas with the remaining area sealed with insulating tapes. For the zinc deposition experiments, an aluminum cathode with 9.8 cm^2 of exposed area was used. A saturated calomel electrode (SCE) connected to a Luggin probe was used to measure the electrode potential. Magnetic stirrers were used to homogenize the solutions with low rotational speed. Cation (H^+ and Zn^{2+}) concentrations were selected to keep the same anion (3 N of chloride or sulfate) concentrations in the both compartments. The solutions in the cathode compartment were designated: (C1) 1.0 M $ZnCl_2$ + 1.0 M HCl; (C2) 0.75 M $ZnCl_2$ + 1.5 M HCl; and (C3) 0.5 M $ZnCl_2$ + 2.0 M HCl. Stock catholyte solutions were made from the reaction of high purity ZnO (>99.99%, Aldrich) and HCl (37%, Aldrich). The catholyte was charged with 1.5 M $ZnCl_2$ solution (pH 4) at every 10 min to keep the zinc concentration in catholyte constant. For levelling deposit surfaces, a 1% gelatin solution was prepared by dissolving gelatin powder (Hopkin & Williams Ltd, Chadwell Heath, Essex, England) in distilled water. The solid content of gelatin was fixed as 80 mg l^{-1} in the catholyte solutions. Electrochemical analysis was conducted in the same electrolysis cell with a Solartron SI 1287, using the zinc cathodes having 1 cm^2 of exposed area. The cathode was connected by a thin and narrow zinc foil (Alrich, 99.99%). Electrolyte resistance between cathode and Luggin probe was measured and ranged between 0.1–0.3 Ω, depending on both the deposit growth and the presence of bubbles on the cathode surface. The IR drop was compensated using a software after the measurements. The composition of the anolyte was measured by AAS (atomic absorption spectroscopy). Acidity of the spent electrolyte was determined by titration with the 0.5 M sodium carbonate solution.

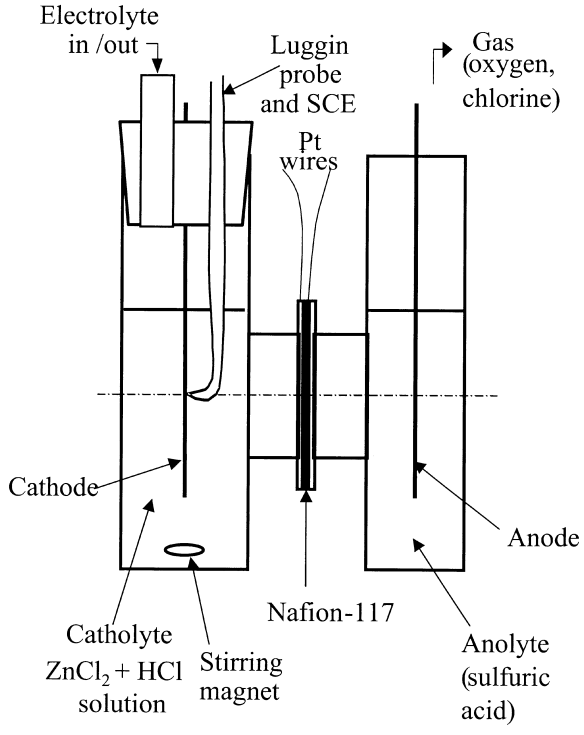

Fig. 1. Schematic of electrolysis cell.

3. Results

3.1. *Electrode potentials*

From the plots of cathode potential against current density in Figure 2, the regions that belonged to the corrosion by HCl and zinc deposition were identified. According to the adion theory [6, 7] of zinc deposition in acidic sulfate solutions, there are two reactions, one is the zinc deposition ($Zn^{2+} + 2\ e^- \rightarrow Zn$) and the other is a hydrogen evolution reaction ($2\ H^+ + 2\ e^- \rightarrow H_2$). These two reactions produce a corrosion process with cathodic reaction ($2\ H^+ + 2\ e^- \rightarrow H_2$) and anodic reaction ($Zn \rightarrow Zn^{2+} + 2\ e^-$). At the corrosion potential or mixed potential (−1.03 V), the dissolution of zinc and the evolution of hydrogen occur at the same rate. The slight deflection at −1.05 V very close to the corrosion potential is due to an increase in electrical resistance between the electrode and the Luggin probe by hydrogen bubble adsorption on the electrode surface. With increasing cathodic overpotential, the adsorbed hydrogen is progressively replaced by the zinc adion, Zn^+_{ad}. Competition exists between the autocatalytic production of the absorbed intermediate Zn^+_{ad} (by the reactions

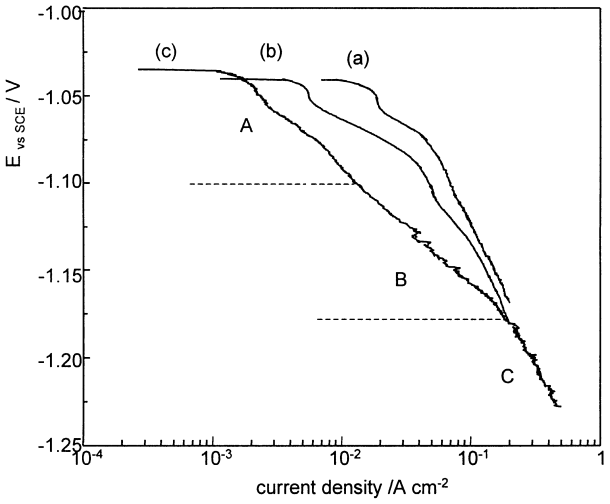

Fig. 2. Plots of cathode potentials (SCE) with current density in 0.5 M $ZnCl_2$ + 2 M HCl at 20 °C and with 0.2 mV s^{-1} scanning rate. (a) polished zinc cathode in gelatin-free solution; (b) polished zinc cathode in gelatin (80 mg l^{-1}) containing solution; (c) zinc deposit grown from C3 solution with gelatin.

$Zn^{2+} + e^- \rightarrow Zn^+_{ad}$ and $Zn^+_{ad} + e^- \rightarrow Zn$) and the adsorption of H^+_{ad} acting primarily as an inhibitor for zinc deposition in the region close to the corrosion potential. In Figure 2, curve (c) exhibits two linear Tafel regions. Assuming a transfer coefficient of 0.5, the lower Tafel slope of about 60 mV in the lower current density region related to zinc deposition, and the higher slope of about 120 mV related to one-electron reaction in the high current density region. In this region, massive hydrogen evolution was visible therefore the one-electron reaction could be related with the hydrogen evolution reaction. The polished zinc cathode showed the narrower range in the current density with the lower Tafel slope. With gelatin addition, the range increased and the deposit grown from C3 solution exhibited the wider range of the linear range.

3.2. *Impedance analysis*

In cathodic polarization region, three types of impedance loops, shown in Figure 3 (designated as A, B and C), were found. The first is near to the corrosion potential and cathodic by less than 50 mV (point A in Figure 2), the second is linear Tafel region with the lower slope (point B), and the third is with the higher slope (point C). The loops in Figure 3(A) show capacitive behaviour only. The high frequency capacitive loop (above 50 Hz) corresponds to the double layer capacitance in parallel with the charge transfer resistance. The lower frequency loop (50–0.5 Hz) corresponds to the adions adsorption and the impedance decreased with increasing the cathodic overvoltage in the A-type region.

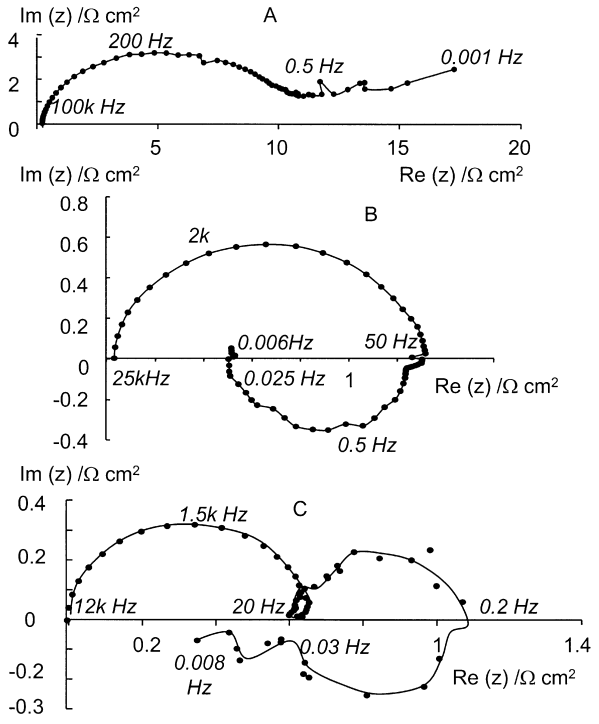

Fig. 3. Impedance plots corresponding to the points in Figure 1(c). (A) 1.07 V vs SCE; (B) 1.15 V; (C) 1.2 V.

The lowest frequency region is also capacitive (below 0.5 Hz) with no inductive behavior being found in this frequency region. The B-type loop was frequently observed in the gelatin containing solutions. High frequency loop is capacitive but the lower frequency region below 50 Hz became inductive. In the region of zinc deposition, the three inductive loops were observed by Cachet and Wiart [8] and respectively reflect, with decreasing the frequency, the relaxation of the electrode coverage by Zn^+_{ad}, ZnH_{ad}, and Zn^*. Zn^* is an active site for nucleation on the surface. The inhibition for the adsorption of ZnH_{ad} was effective; thereby the hydrogen evolution reaction could be suppressed in the B-type region. In the C-type domain, the impedance curve has one inductive loop at lowest frequency range and two capacitive loops, one corresponding to Zn^+_{ad} (about 10–50 Hz), the other to ZnH_{ad} (about 0.1–10 Hz), were observed. Massive hydrogen evolution was observed in the C-type region.

The adsorption or inhibition tendency was found to be dependent on the surface conditions of electrodes. As shown in Figure 2, the B-type domain was widened until above 100 mA cm^{-2} in the case of the deposit having a strongly developed (1 1 0) preferred texture while other cathodes polished on abrasive papers (2400 grit) changed to C type above 50 mV cm^{-2}.

3.3. *Current efficiency*

In this experiment, high cathodic current density was intentionally avoided to decrease the cell voltage. However, CE dependence on the current density is worthy of consideration. Without gelatin, lower efficiencies resulted, for example, 90% from C2 and 77% from C3. As shown in the Table 1, gelatin addition improved the CE significantly. In C3 solution, the efficiency increased from 77% to 95% by gelatin addition. The gelatin effect becomes weak at high temperature (>40 °C) since it may be degraded in the bulk solution rather than adhering on the cathode.

3.4. *Deposit morphology*

The description of the deposits is listed in Table 1. Without gelatin, all the deposits in the solutions showed the rough and porous appearances. As shown in Figure 4, a very porous microstructure morphology was observed. In Figure 4(a) the coarse zinc particles are connected one another but if it is magnified to see the each particle as in Figure 4(b) and (c), very fine surface protrusions are shown.

Gelatin as a levelling agent was found effective for Zn deposition in the solutions. Without air sparging, and with mild stirring only, dense and flat deposits resulted. The deposit from solution C2 shown in Figure 5, had a fine and dense surface morphology. The coating was equiaxed but was found slightly oriented towards the (1 0 1) plane by XRD analysis. Such a preferred texture could be removed by polishing the coating, and exhib-

Table 1. Current efficiency in Zn electroplating in zinc chloride and hydrochloric acid solutions

Catholyte*	Temp. /°C	Current density at cathode /mA cm^{-2}	Gelatin /mg l^{-1}	CE /%	Morphology	Preferred texture
C1	25	50	80	98	dense	random
C2	25	50	No	90	porous and dendritic	random
C2	25	50	80	97	dense	(1 0 1), (1 0 3)
C3	25	50	No	77	porous and nodular	(0 0 2), (1 0 3)
C3	25	50	80	96	columnar	(1 1 0)
C3	35	50	80	91	columnar and nodular	(1 1 0)
C3	40	50	80	85	columnar and nodular	(1 1 0) $\gg$ (1 0 1)
C3	25	100	80	91	columnar and nodular	(1 1 0) > (1 0 1)

* C1: 1 M $ZnCl_2$ + 1 M HCl.
C2: 0.75 M $ZnCl_2$ + 1.5 M HCl.
C3: 0.5 M $ZnCl_2$ + 2 M HCl.

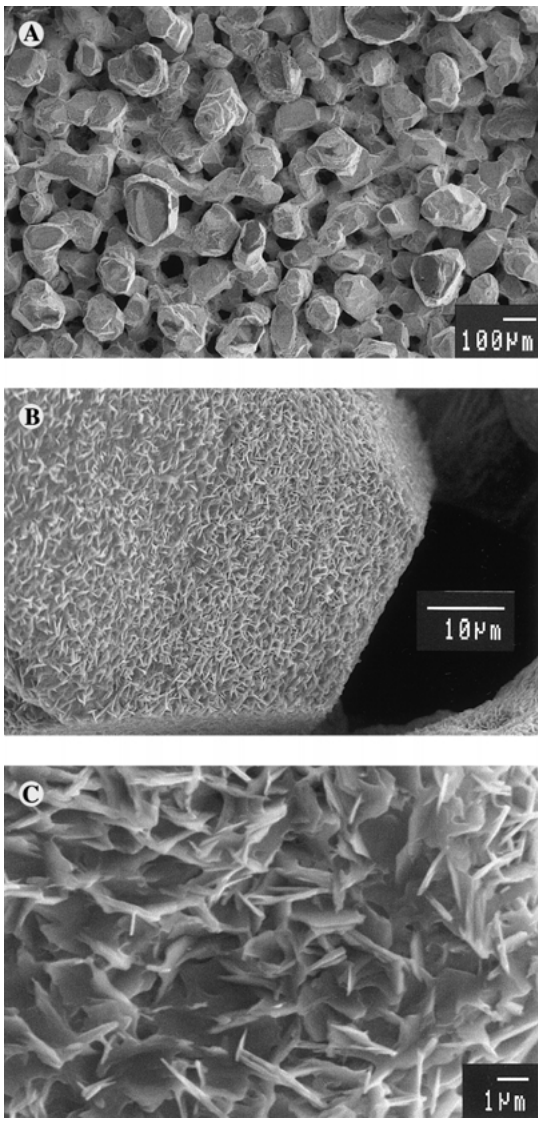

Fig. 4. Morphology of deposits from the gelatin-free solution (0.5 M $ZnCl_2$ + 2 M HCl) showing the fine protrusions on the surface. (A) Surface morphology of deposit; (B) and (C) magnified views.

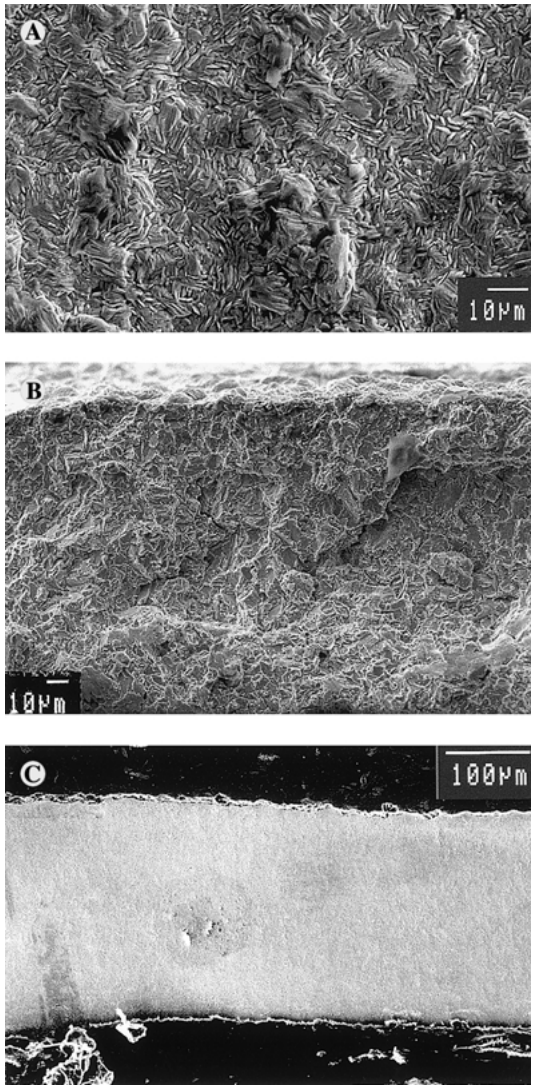

Fig. 5. Morphology of deposits from the gelatin containing solution (0.75 M $ZnCl_2$ + 1.5 M HCl). (A) Surface morphology of deposit; (B) fractured surface; (C) cross-sectional view of polished and etched specimen in 1 M HNO_3.

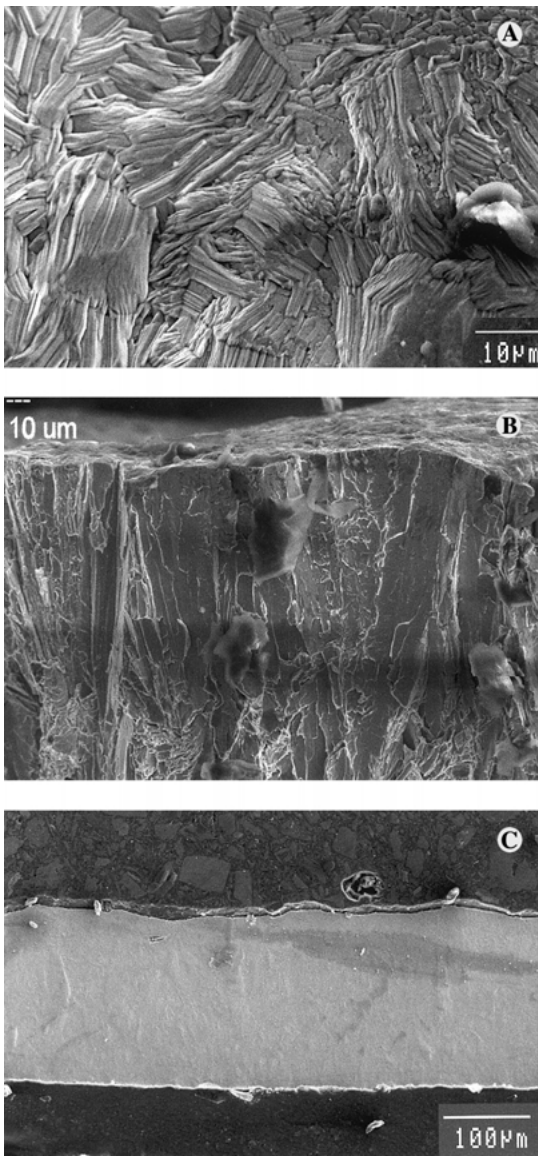

Fig. 6. Morphology of deposits from the gelatin containing solution (0.5 M $ZnCl_2$ + 2 M HCl). (A) Surface morphology of deposit; (B) fractured surface; (C) cross-sectional view of polished and etched specimen in 1 M HNO_3.

ited an almost same pattern with JCPDS data. Pores were not observed in the polished surfaces from the top-view. The cross-sectional view of the coating shows the flat and dense appearance. The deposit from C3 (Figure 6) also showed a dense structure but with sparsely scattered dents (observed from the top-view). The coating had a lustrous and glossy surface while other deposits from C1, and C2 showed nonlustrous surfaces.

X-ray diffraction analysis showed a difference in the crystallographic orientation of the deposits (Figure 7). As described in Table 1, a strong preferred texture of (1 1 0) was observed. From the observation of the fractured surface (Figure 6(b)), the texture was resulted from a unidirectional growth. The bottom of the deposit looks equiaxed and the preferred texture is more significant with the thickness (i.e., deposition time).

4. Discussion

4.1. *Hydrogen evolution*

For evolution of hydrogen from Zn surfaces where Zn electrodeposition is predominant, reactions including the adsorption of hydrogen ion ($H^+ + e^- + Zn \rightarrow ZnH_{ad}$) and the desorption of hydrogen gas from the zinc surface ($ZnH_{ad} + H^+ + e^- \rightarrow Zn + H_2$) take place [9]. As suggested by R. Ichino et al. [10] hydrogen ion may be adsorbed at active sites ($H^+ + e^- + Zn^* \rightarrow ZnH_{ad}$) related with Zn nucleation and then released as a hydrogen gas. The nucleation sites are more abundant on fine and random oriented zinc surfaces than unidirectionally grown large crystalline surfaces. The hydrogen ion is preferentially adsorbed on the nucleation sites than onto the uniformly stacked crystalline surface. Accordingly, the high CE is the result of the preferred texture of the deposit that has less defects and grain boundaries providing nucleation sites for H_2 gas evolution. It was possible to see the difference between the bubble sizes formed on the cathodes. The deposits with random orientation produced fine bubbles quickly floating up while the deposit with the preferred texture formed large bubbles adhering on the surface long time. Another consideration for high CE in B-type domain is due to the inhibition of the hydrogen adsorption process by gelatin molecule. It is probable that the molecule is more preferentially adsorbed on the nucleation or protrusion sites because of their higher electrical field intensity.

4.2. *Morphological effect on the current density*

Mackinnon and Brannen [11] suggested that using excess glue gave a higher overpotential and (1 1 0) orientation. The morphological transition, from (0 0 2) to (1 1 0) in accordance with overvoltage, may be applied in this experiment. The deposit from C3 without gelatin shows a weakly (0 0 2)-preferred texture. Some deposits exhibited the intermediate orientations (1 0 1) and (1 0 3) as shown in the Table 1. A systematic relationship between the overpotential and the orientation was not observed. According to the Table 1, the CE is related to the preferred orientation of (1 1 0) as current efficiency increases with the tendency of (1 1 0) orientation.

The coating obtained from C3 with gelatin could be easily separated from aluminium cathode but easily broken by bending as reported in the case of sulfate electrolysis by Robinson and O'Keefe [12]. In chloride electrolysis, Thomas and Fray [4] also used glycine, one of the amino acids constituting gelatin, but did not report the (1 1 0) orientation. The microstructures in both these cases had columnar structures that are very similar to the structure from C3 containing gelatin. It is also possible to understand that gelatin may coat some zinc planes and prevent further growth. However, the (1 1 0)-preferred texture is not unique to gelatin.

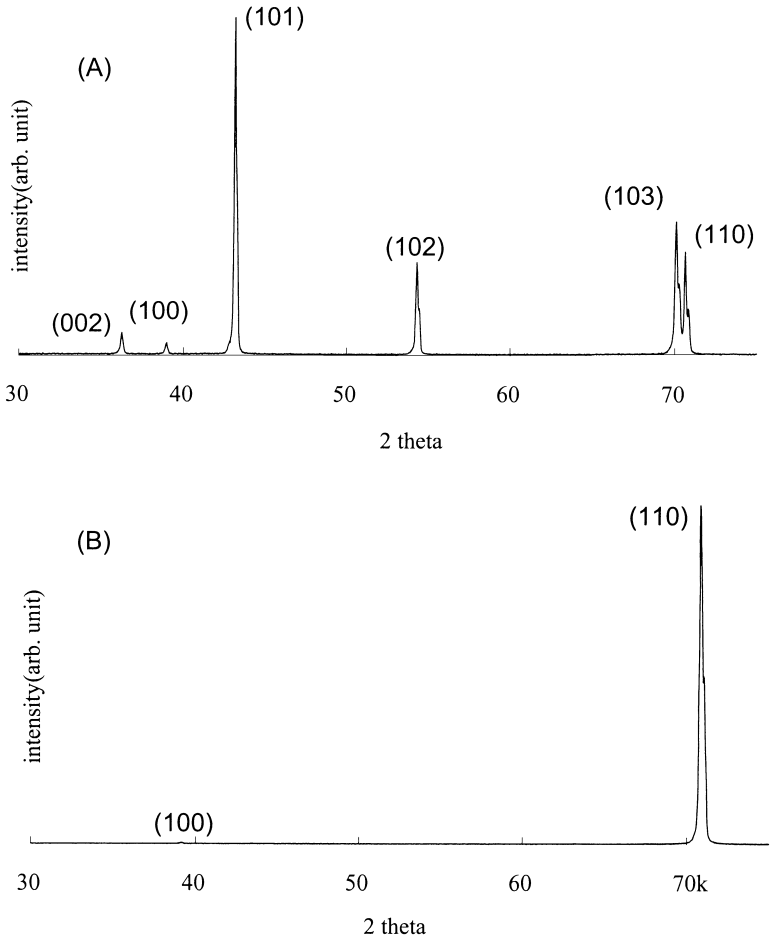

Fig. 7. X-ray diffractograms of deposits grown from gelatin-containing solutions. (A) 0.75 M $ZnCl_2$ + 1.5 M HCl, corresponding to Figure 5 (B) 0.5 M $ZnCl_2$ + 2 M HCl, corresponding to Figure 6.

Table 2. Corrosion current and Tafel slopes of the Zn cathode materials

Cathode	Solution, gelatin concentration	Corrosion potential E_c /V vs SCE	Polarization resistance R_p /Ω cm^2	Bc (Tafel slope) in the range of current density /mA cm^{-2}	Corrosion current I_c /mA cm^{-2}
Polished zinc*	C3, free	−1.022	1.58	0.14 (>60)	16.4
Polished zinc*	C3, 80 mg l^{-1}	−1.013	6.64	0.15 (100–150)	3.9
Random oriented deposit (microstructures in Figure 4)	C3, 80 mg l^{-1}	−1.021	6.27	0.08 (10–100) 0.165 (>150)	4.1
(1 1 0)-oriented deposit (microstructures in Figure 5).	C3, 80 mg l^{-1}	−1.019	12.69	0.066 (10–100) 0.133 (>150)	2.0

* Polished zinc (zinc foil 99.99%, Aldrich) is prepared by polishing on 2400 grit abrasive paper.

Mackinnon and Brannen [13] found tetrabutylammonium chloride and tetrapentylammonium chloride produced (1 1 0) texture.

The surface diffusion of the adsorbed molecules and the bulk diffusion flux of cations to the surface characterize the number density of the steps on the electrode surface. Zinc crystal grows mainly in the direction parallel to (0 0 1) plane and also in the perpendicular to the plane with the addition of new steps. Accordingly, when the formation rate of the steps is not enough for the zinc ion discharge, the preferential growth in the direction (1 1 0) results.

4.3. *Relation with corrosion characteristics*

To compare the degrees of imperfections that may be the sites for H_2 evolution, corrosion currents between the cathodes were measured. Although the corrosion current as compared to the total current is very small at the deposition potential, the corrosion characteristics of the deposits may be an indirect means of comparing surface defects. Using the potential–current curves, the polarization resistances near the corrosion potential were used to calculate corrosion currents by Stern and Geary's formula [14]. Corrosion current densities for the

deposits with random orientation and with (1 1 0) preferred texture were 4.1 and 2.0 mA cm^{-2}, respectively. It is interesting that the polished Zn cathode tested in the gelatin containing C3 exhibited the significant decrease in the corrosion current, in comparison with the value obtained in the gelatin free solution. The corrosion behaviour of zinc is known to be dependent upon the texture. Park and Szpunar [15] showed that the corrosion resistance of zinc coating increased with the basal texture (0 0 1) following the concept that the close packed planes were more resistant to dissolution because of the higher binding energy of the surface atoms. Some investigations [16, 17] in neutral or alkaline solutions also suggested that the (1 1 0) plane had the highest corrosion rate. Accordingly, the corrosion resistance and the CE of the deposit are more dependent on the surface imperfection than the texture orientation.

5. Conclusions

High current efficiency was attained from the electrolysis in 2 M HCl and 0.5 M $ZnCl_2$, which was enough for the leaching of zinc concentrates. Although CE for zinc deposition decreased with high HCl concentration, the introduction of an inhibitor such as gelatin for H_2 evolution process significantly improved the CE. The gelatin layer may decrease the H^+ adsorption on the active Zn sites and increase the current efficiency. It was found the high efficiency was related to the preferred texture (1 1 0) of the deposits having relatively fewer imperfections on the crystal surface.

References

1. G.P. Demopoulos, *Can. Metall. Quart.* **37**(1) (1998) 1.
2. B.K. Thomas and D.J. Fray, *Trans. Instn Min. Metall.* Sect. C **91** (1982) C105.
3. L. Liao, A.V. Sandwijk, G.V. Weert and H.W. De Wit, *J. Appl. Electrochem.* **25** (1995) 1009.
4. B.K. Thomas and D.J. Fray, *J. Appl. Electrochem.* **11** (1981) 677.
5. A.E. Saba and A.E. Elsherief, *Hydrometallurgy* **54** (2000) 91.
6. R. Ichino, C. Cachet and R. Wiart, *Electochimica Acta* **41** (1996) 1031.
7. C. Cachet and R. Wiart, *J. App. Electrochem.* **20** (1990) 1009.
8. C. Cachet and R. Wiart, *J. Electrochem. Soc.* **141** (1994) 131.
9. J. Bressen and R. Wiart, *J. App. Electrochem.* **9** (1979) 43.
10. R. Ichino, C. Cachet and R. Wiart, *Electrochim. Acta* **41** (1996) 1031.
11. D.J. Mackinnon and J.M. Brannen, *J. App. Electrochem.* **7** (1977) 451.
12. D.J. Robinson and T.J. O'Keefe, *J. Appl. Electrochem.* **6** (1976) 1.
13. D.J. MacKinnon and J.M. Brannen, *J. App. Electrochem.* **12** (1982) 21.
14. M. Stern and A.L. Geary, *J. Electrochem. Soc.* **104** (1957) 56.
15. H. Park and J.A. Szpunar, *Corros. Sci.* **40** (1998) 525.
16. D. Abayarathan, E.B. Hale, T.J. O'Keefe, Y.M. Wang and D. Radovic, *Corros. Sci.* **32** (1991) 755.
17. R. Guo, F. Weinburger and D. Tromans, *Corrosion* **51** (1995) 356.